International Journal of Biological Macromolecules 199 (2022) 372–385

Contents lists available at ScienceDirect

International Journal of Biological Macromolecules

journal homepage: www.elsevier.com/locate/ijbiomac

Fabrication of cellulose nanocrystals as potential anticancer drug delivery systems for colorectal cancer treatment

Mostafa Yusefi [a], Michiele Lee-Kiun Soon [b], Sin-Yeang Teow [b,*], Elaine Irene Monchouguy [b], Bibi Noorheen Haleema Mooneerah Neerooa [b], Zahra Izadiyan [a], Hossein Jahangirian [c], Roshanak Rafiee-Moghaddam [c], Thomas J. Webster [c], Kamyar Shameli [a,*]

[a] Malaysia-Japan International Institute of Technology, Universiti Teknologi Malaysia, Jalan Sultan Yahya Petra, Kuala Lumpur, Malaysia
[b] Department of Medical Sciences, School of Medical and Life Sciences, Sunway University, Jalan Universiti, Bandar Sunway, Selangor Darul Ehsan, Malaysia
[c] Department of Chemical Engineering, College of Engineering, Northeastern University, Boston, United States of America

ARTICLE INFO

Keywords:
Natural polysaccharide
Drug loading
pH sensitivity
Anticancer activity

ABSTRACT

Polysaccharide nanocrystals have great potential to be used as improved drug carriers due to their low cost, high biodegradability, and biocompatibility. This study reports the synthesis of cellulose nanocrystals (CNC) loaded with 5-fluorouracil (CNC/5FU) to evaluate their anticancer activity against colorectal cancer cells. X-ray and Fourier-transform infrared spectroscopy demonstrated that acid hydrolysis successfully degraded the amorphous cellulose to liberate the crystal regions. From transmission electron microscopy, CNC/5FU appeared as rod-like nanocrystals with an average length and width of 69.53 ± 1.14 nm and 8.13 ± 0.72 nm, respectively. The anticancer drug 5FU showed improved thermal stability after being loading onto CNC. From UV–vis spectroscopy data, the drug encapsulation efficiency in CNC/5FU was estimated to be 83.50 ± 1.52%. The drug release of CNC/5FU was higher at pH 7.4 compared to those at pH 4.2 and 1.2. From the cytotoxicity assays, CNC did not affect the viability of CCD112 colon normal cells. On the other hand, CNC/5FU exhibited anticancer effects against HCT116 and HT-29 colorectal cancer cells. The anticancer actions of CNC/5FU against HCT116 cells were then confirmed using an in vitro tumor-on-chip model and clonogenic assay. Mechanistic studies demonstrated that CNC/5FU killed the cancer cells by mainly inducing cell apoptosis and mitochondrial membrane damage. Overall, this study indicated that CNC/5FU could be a potential nanoformulation for improved drug delivery and colorectal cancer treatment.

1. Introduction

Using innovative materials with desirable characteristics can overcome many of the global health risk issues in the present time. Biopolymers have several significant features for improved drug delivery linked to developing advanced technologies to promote a healthy society. In this manner, the therapeutic nature of nanomaterials with an arsenal of drug delivery systems has several advantages over conventional cancer therapy methods due to their low damage to normal cells and ability to deliver sufficient drug dosages to a tumor [1]. To date, the U. S. Food and Drug Administration (FDA) has approved five such nanocarriers, including liposomes, albumin nanoparticles (NPs), and polymeric micelles [2]. Natural polymers have taken advantage of improved biocompatibility for drug delivery applications to possibly replace most of the current nonbiodegradable polymers [3,4].

The association of nanotechnology with biomedical science is currently gaining momentum as innovative and complementary therapeutic modalities for treating cancer in clinical trials [5]. Numerous innovative anticancer agents and chemotherapeutic approaches are continuously being discovered and effectively exploited in cancer therapy to prolong the life span of cancer patients [6,7]. Despite this, chemo-drugs possess issues of morbidity and harmful side-effects due to their lack of bioavailability and consequent high-doses [8]. In addition, many chemo-drugs are poorly water-soluble that can cause a poor and heterogeneous distribution of drugs in tumors and thereby therapeutic failure. The disadvantages of chemotherapy might be alleviated by loading a sufficient dosage of chemo-drugs, such as 5-fluorouracil (5FU), onto various polymer and polysaccharide-based carrier systems, for

* Corresponding authors.
E-mail addresses: ronaldt@sunway.edu.my (S.-Y. Teow), kamyar@utm.my, kamyarshameli@gmail.com (K. Shameli).

https://doi.org/10.1016/j.ijbiomac.2021.12.189
Received 29 September 2021; Received in revised form 14 December 2021; Accepted 29 December 2021
Available online 6 January 2022

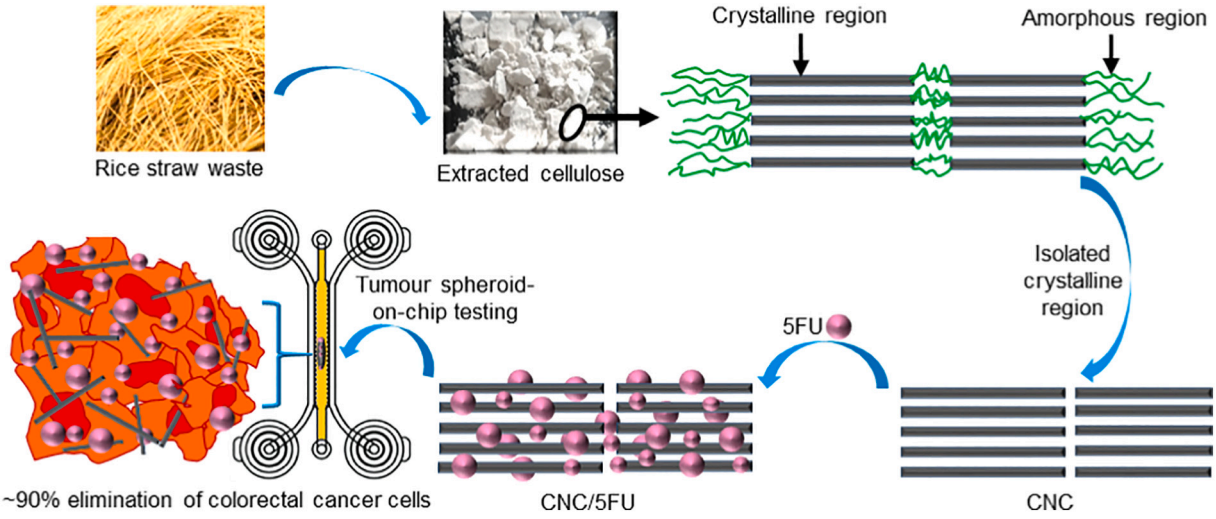

Scheme 1. (A) The schematic procedures for CNC/5FU fabrication for in vitro anticancer analysis towards colorectal cancer cells. (B) The possible intermolecular chemical interactions between active functional groups in CNC/5FU.

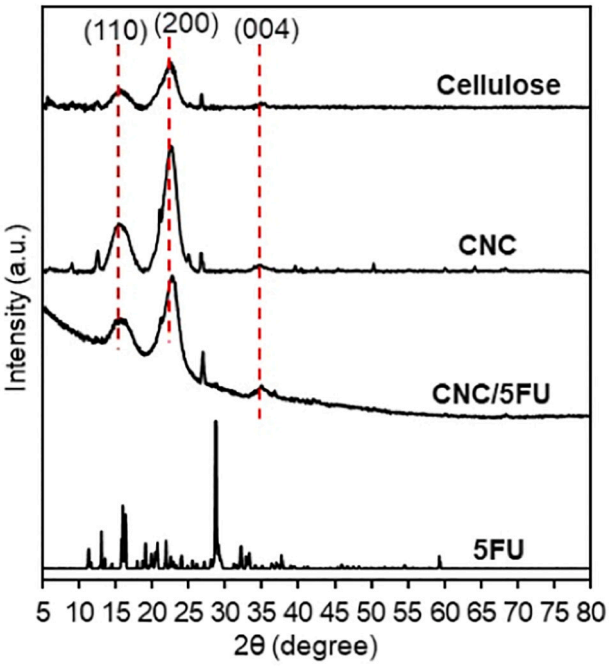

Fig. 1. XRD results of cellulose, CNC, CNC/5FU, and 5FU.

instance, poly(2-vinyl pyridine)-b-poly(ethylene oxide) nanomicelles [9], chitosan microspheres [10,11], carboxymethyl cellulose [12], and cellulose nanocrystals (CNC) to name a few [13].

With the immense demand for using biocompatible nanocarriers in anticancer drug delivery systems, CNC as a type of polysaccharide should be explored as a treatment for killing cancer cells [14]. CNC with a desirable structure, improved crystallinity or ordered regions, and also nano-dimensional scale can be isolated from various wood-based materials, such as rice straw waste [15]. It has been also termed nanocrystalline cellulose (NCC) and cellulose nanowhiskers (CNW) [16]. CNC and CNC-based products possess desirable properties, including the capability to bind with various drugs, great swelling behavior, pH gradient behavior, and high biodegradability for innovative antitumor drug delivery systems [17]. Each property has its particular pros and cons for developing a topical nanodrug formulation with improved stability and therapeutic effects [18]. The vitality of drug-loaded CNC is a consequence of its potential to deliver a desirable amount of drugs to cancer cells without significant effects against normal cells to possibly decrease medical malpractice derived from the drug alone [18,19]. For example, curcumin was loaded onto CNC and caused almost three times higher colorectal cancer cell death than that of curcumin alone [20]. Gao et al. in a different report used rice husk to extract acid hydrolyzed CNC and then analyzed its phytochemical bioactivities [15]. However, there have been no comprehensive studies on the anticancer drug-loaded CNC properties obtained from rice straw waste and its associated anticancer applications.

This present research aimed to fabricate 5FU-loaded CNC for in vitro anticancer analysis. The fabricated samples were analyzed by various characterization techniques. Drug encapsulation efficiency and drug release were also examined. The biocompatibility and anticancer effects of CNC and the 5FU-loaded CNC were studied using colon normal (CCD112) and colorectal cancer (HCT116 and HT-29) cells with an in vitro tumor-on-chip model and clonogenic assay.

2. Methodology

2.1. Materials

Potassium hydroxide (KOH, 85%, EM Science), sodium chlorite ($NaClO_2$, 80%, Fluka), acetic acid (CH_3COOH), and sulfuric acid (H_2SO_4, 95–98%, ACS GR, EMD) were purchased from Sigma-Aldrich (St Louis, MO, USA). The anticancer drug 5FU (99%, 5-Fluoro-2,4(1H,3H)-pyrimidinedione (ACD CODE MFC D00006018) with molecular weight of 130.08 g/mol) was purchased from Acros Organics (Thermo Fisher Scientific, New Jersey, USA).

2.2. Preparation of cellulose nanocrystals (CNC)

Cellulose from rice straw waste was obtained as described previously [21]. The powder from rice straw waste was mixed with toluene/ethanol 2:1 (*v*/v) and placed in a Soxhlet instrument for 12-h at 70 °C. This was followed by mixing the dewaxed rice straw with NaCl (1.4%) and CH_3COOH, at pH 4 and 70 °C for 5-h. After washing the sample, a potassium hydroxide solution (5%) was used to treat the sample for 12-h. The natural cellulose solution was centrifuged and freeze-dried (FreeZone 1.0 L Benchtop Freeze Dry System) at −45 °C for 48-h. The obtained cellulose was mixed with a H_2SO_4 solution (64% *w*/w) at a ratio of 1:2 for 5-min, and the hydrolysis process was quenched by placing the sample solution into an ice water bath. The nanocrystal gel was

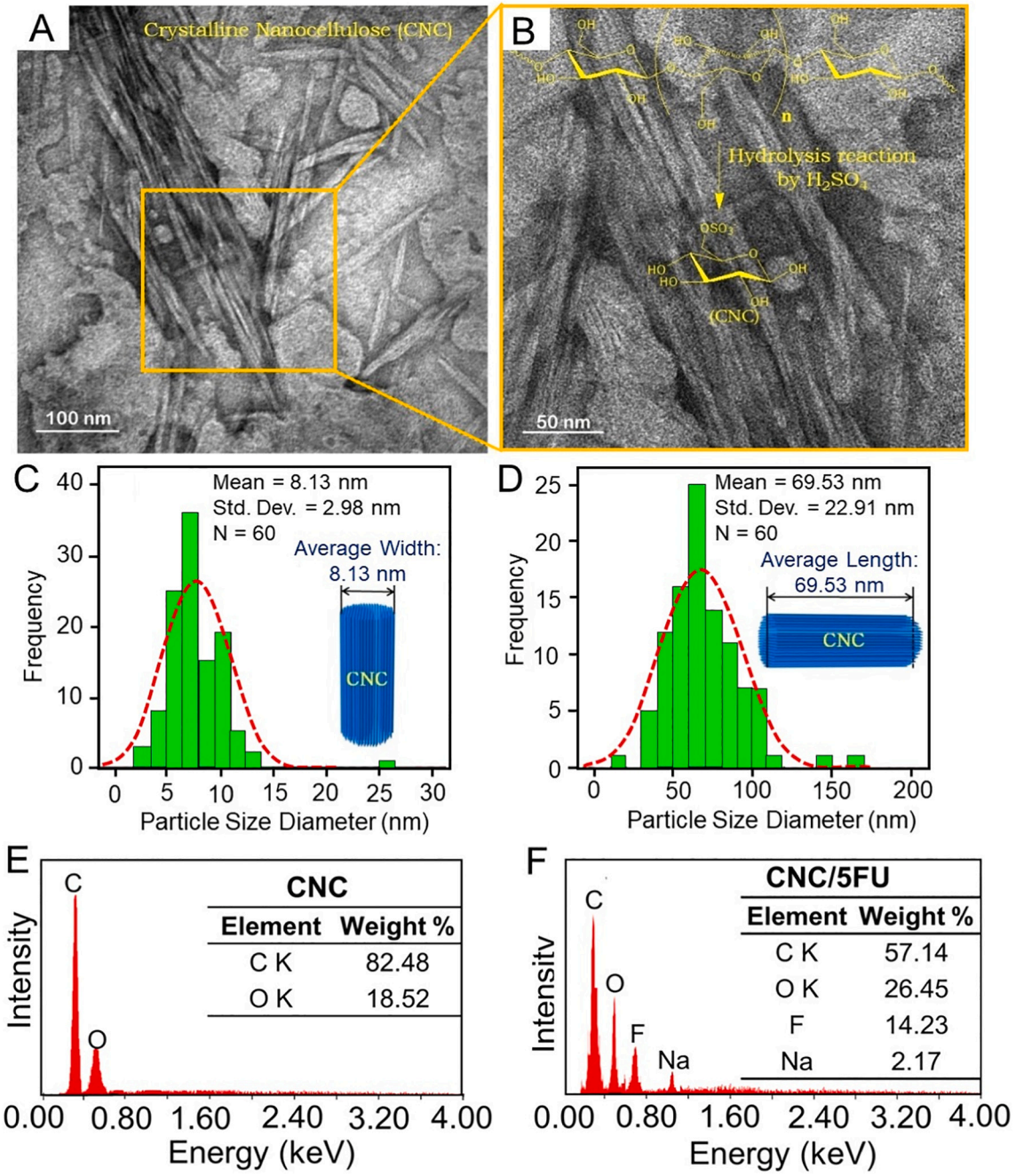

Fig. 2. (A) and (B) TEM images of CNC/5FU, the average (C) width and (D) length of CNC/5FU. EDX of (E) CNC and (F) CNC/5FU.

subsequently ultrasonicated for 10-min at a 20% amplitude (Misonix ultrasonic) in an ice bath. The CNC solution was centrifuged and freeze-dried at −45 °C for 48-h and stored at 4 °C for further analysis.

2.3. Fabrication of CNC/5FU and drug loading study

5FU and CNC powder at a weight ratio of 1:3.5 was mixed with distilled water under 300 rpm magnetic stirring for 14-h. Then, the CNC/5FU solution was centrifuged and freeze-dried at −45 °C for 48-h. To measure the unloaded drug, the obtained supernatant was evaluated via UV–vis spectrophotometry at λ_{max} = 266 nm using a calibration curve obtained from various concentrations of 5FU to measure loading capacity (LC) based on Eq. (1) [22]:

$$LC\ (\%) = \frac{(Initial\ drug\ amount\ in\ formulation\ (mg) - Unentrapped\ drug\ (mg))}{Total\ weight\ of\ sample\ (mg)} \times 100 \quad (1)$$

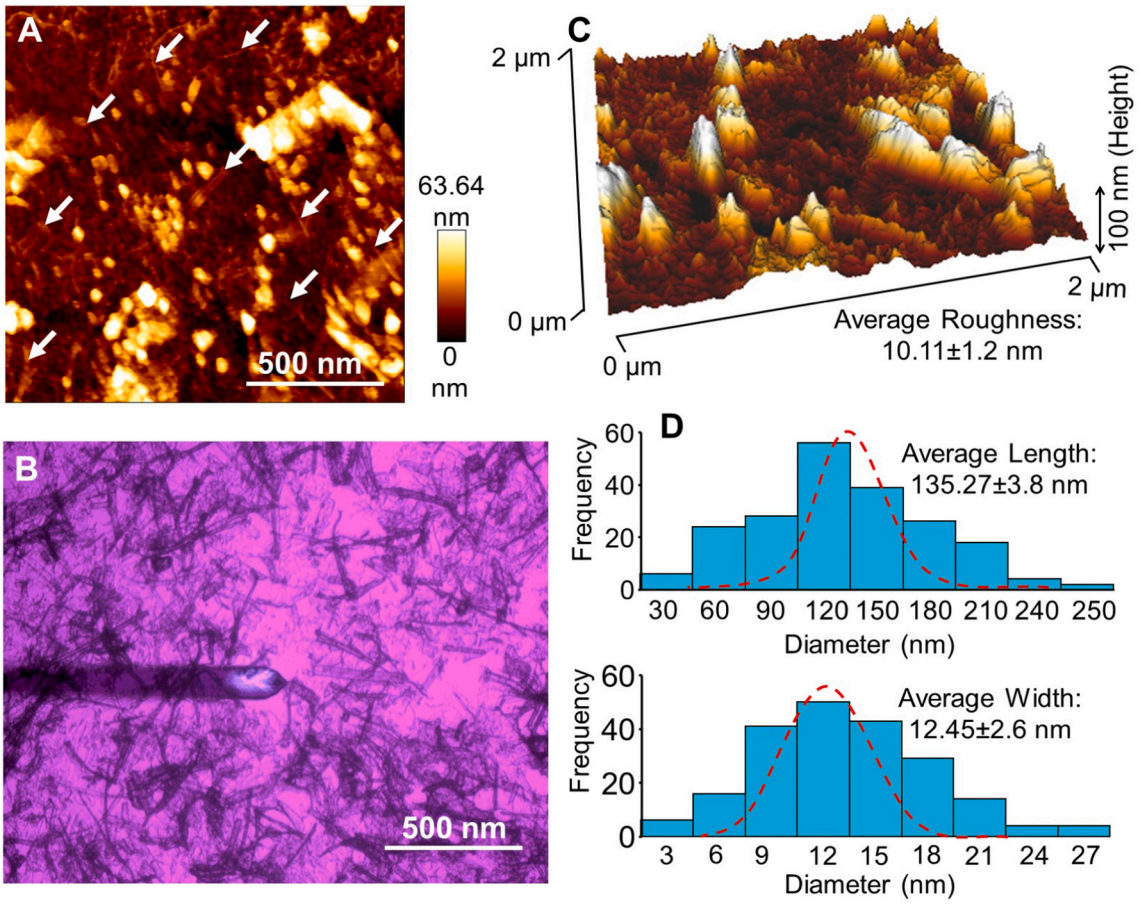

Fig. 3. Representative AFM (A) images of vertical deflection, (B) 2D image (C), 3-D surface height profiles, and (D) histograms of the obtained diameters of CNC/5FU.

The encapsulation efficiency (EE) was calculated following Eq. (2) [23]:

$$\text{EE}\ (\%) = \frac{(\text{Initial drug amount in formulation (mg)} - \text{Unentrapped drug (mg)})}{\text{Initial drug amount in formulation (mg)}} \times 100 \quad (2)$$

2.4. Physicochemical characterization of CNC/5FU

X-ray powder diffraction (XRD) (Philips, X'pert, Cu Ka) at room temperature was utilized to characterize crystallinity, by which the analysis was accomplished using dispersion 2 theta angles of 5°–80° with a scanning rate of 2 s/step, voltage of 45 kV, a Ni-filtered Cu K radiation (=1.5406 A)°, and a filament current of 40 mA (Philips, X'pert, Cu Ka). The crystallinity index of CNC was measured using Eq. (3):

$$\text{Crystallinity index}\ (\%) = \frac{A_{\text{crystalline}}}{A_{\text{amorphous}} + A_{\text{crystalline}}} \times 100 \quad (3)$$

where $A_{\text{amorphous}}$ and $A_{\text{crystalline}}$ are the area below the amorphous curve and the sample curve, respectively.

The crystal CNC size was estimated using Scherrer's equation (Eq. (4)) [24]:

$$\text{Crystal size L} = \frac{k\lambda}{\beta}\cos\theta \quad (4)$$

where λ = 0.1540 nm, k is the correction parameter of 0.91, θ = diffraction angle in radians, and β = full width at half maximum.

The d spacing of the cellulose was analyzed using Bragg's law as calculated by Eq. (5):

$$d = n\lambda/(2\ sin\ \theta) \quad (5)$$

where d is the interplanar distance between lattice planes, θ is the scattering angle in degrees, n is a positive integer and λ is the wavelength of the X-ray [25].

In TEM analysis, a drop of a solution of CNC/5FU and distilled water (ratio 0.005, *w*/w%) was placed onto glow-discharged carbon-coated TEM grids (300-mesh copper, formvar-carbon, Ted Pella Inc., Redding, CA) and the extra liquid was wiped by soaking up a piece of filter paper (Whatman filter) after 3-min. A 2% uranyl acetate solution was used to negatively stain the samples for 3-min, followed by wiping the extra liquids and drying at room temperature. TEM images of the samples were obtained by a Philip CM12 TEM performed at a 100 kV

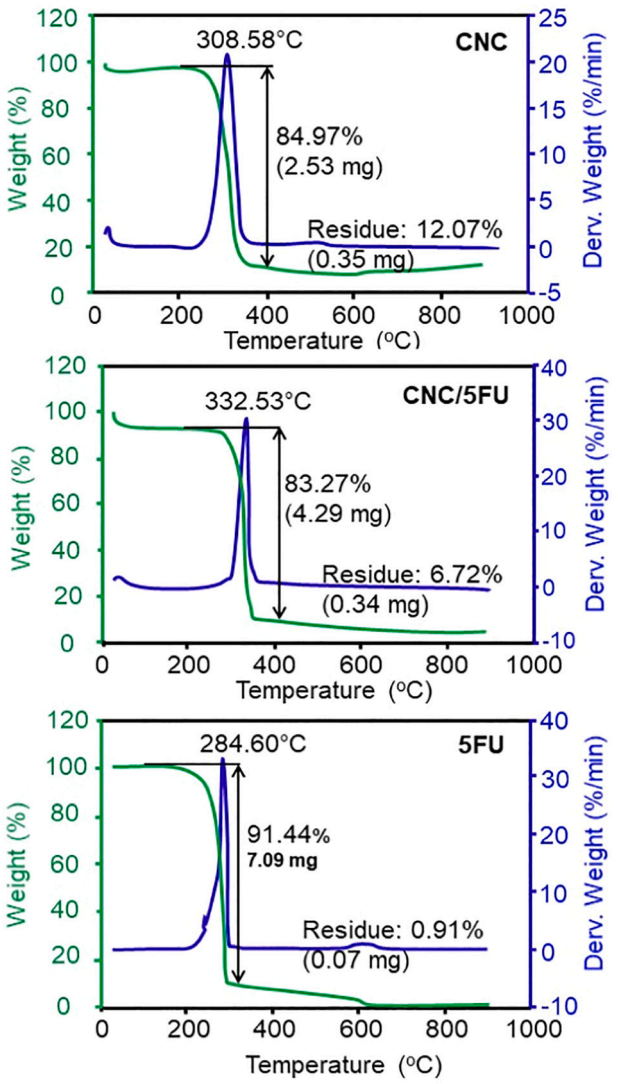

Fig. 4. TGA and DTGA traces of CNC, CNC/5FU, and 5FU.

accelerating voltage. From the obtained TEM images, the average width and length of the samples were calculated from around 60 individual CNC/5FU by analySIS FIVE and Origin Pro software. EDX analysis was carried out using the chamber at 5 Torr with the condenser lens setting at 40%. AFM was performed by tapping mode and a Veeco nanoscope iiia atomic force microscope (USA) at room temperature. A drop of a diluted aqueous suspension of CNC/5FU (0.0005% *w*/w with distilled water) was sonicated for 2-min and dispersed on the surface of an optical glass substrate and dried under a desiccator at room temperature. The height of 60 CNC/5FU particles was measured and the average width and length of the samples were calculated from around 60 individual CNC/5FU by analySIS FIVE and Origin Pro software. Thermal analysis was performed by using thermogravimetric analysis (TGA) (STA F3 Jupiter, Q50 V20) at a heating rate of 10 °C/min under a nitrogen atmosphere. For Fourier-transform infrared (FTIR) spectroscopy (ThermoNicolet, Waltham), the sample at a ratio of 1:100 *w*/w was mixed with KBr to prepare a transparent pellet which was analyzed under transmittance mode in a range between 4000 cm^{-1} to 400 cm^{-1} with a 4 cm^{-1} resolution and an accumulation of 128 scans. Dynamic light scattering (DLS) was carried out using an Anton Paar instrument (Litesizer 500) to measure zeta potential and hydrodynamic particle size of the sample in a phosphate-buffered saline (PBS) solution (80 mL; 100 μg/mL) at pH 7.4 and 37 °C immediately post-synthesis and subsequently after 1, 2, 3, and 4 weeks of storage.

For the swelling analysis, the sample was immersed in PBS at pH 7.4 and 37 °C. At each interval, the sample was collected from the solution and blotted on a filter paper to eliminate excess water and it was immediately weighed to determine the weight of the wet sample using the equation of W_t/W_0, in which W_t and W_0 are the obtained wet weights at the arbitrary and initial time, respectively. The same swelling experiments were performed for CNC and CNC/5FU in a hydrochloric acid (HCl) solution at pH 4.2 and 1.2.

2.5. In vitro drug release

The UV absorbance (UV-1600, Shimadzu, Japan) of 5FU at five different concentrations (1.0–5.0 μg/mL) was evaluated at $\lambda_{max} = 266$ nm [26]. Before the experiment, the dialysis bag (molecular weight cut-off between 12 and 14 kDa) was soaked in PBS at pH 7.4. The solution mixture consisting of 5 mg CNC/5FU and 2 mL of release media was suspended in the bag with two ends tied which then was immersed into 40 mL of release media maintained at 37 °C in a stoppered bottle under 75 rpm magnetic stirring. A 1 mL aliquot was withdrawn from the system at the selected time point followed by UV–vis spectrophotometry measurements. The 5FU release procedure was continued until the absorbance of the medium remained constant after 36-h. The same study was performed in the HCl solution at pH 1.2 and 4.2, respectively. A comparison of the differences in the drug release profiles was estimated from CNC/5FU in media at various pH values and was calculated by the following equation (Eq. (6)) [26]:

$$\text{Drug release } (\%) = \frac{\text{Amount of drug release at time't'}}{\text{Amount of drug release at time} = 0} \times 100 \quad (6)$$

2.6. Cell lines and reagents

Human HCT116 (ATCC CCL-247), HT-29 (ATCC HTB-38), and CCD112 colon fibroblast (ATCC CRL-1541) cell lines were purchased from ATCC and cultured according to the ATCC's recommendation [27]. The cell lines were maintained in Dulbecco's Modified Eagle's medium (DMEM) supplemented with 10% fetal bovine serum (FBS) (Gibco) and 1% penicillin/streptomycin (Gibco).

2.7. In vitro anticancer assays

The anticancer effects of CNC and CNC/5FU were determined in both 2D monolayer and 3D spheroid models. 5FU was used as the positive control. Cytotoxicity assays on the 2D monolayer was performed using a CellTiter-Glo 2.0 Luminescent Cell Viability Assay (#G9241, Promega), according to the manufacturer's instruction with slight modification as previously described [27]. Briefly, 5000 cells per well (100 μL/well) were seeded onto a 96 well plate and incubated overnight at 37 °C in a 5% CO_2, 95% humidified incubator. The next day, 2-fold serially diluted samples at concentrations of 0, 7.81, 15.62, 31.25, 62.53, 125, 250, and 500 (100 μL/well) were added into the wells and the plate was incubated for 72-h at 37 °C in the 5% CO_2 incubator. Then, 100 μL of the reagent per well was added into the plate and incubated for 30-min at 37 °C in the 5% CO_2 incubator before the plate was read using a multimode microplate reader (Tecan). For the 3D tumor model, an inhibition assay was performed as previously described [28]. 100 μL of 1 $\times 10^4$ colon cancer cells were seeded onto a sterile CellCarrier Spheroid ultra-low attachment 96-well microplate (#6055330, Perkin Elmer) to

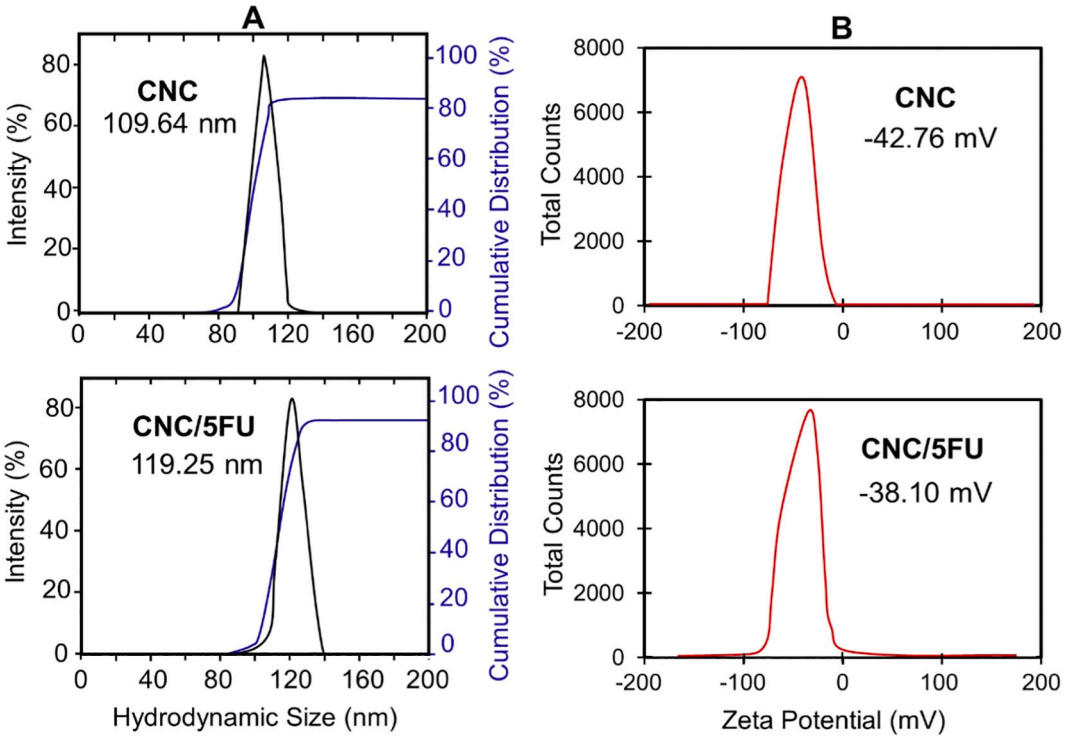

Fig. 5. (A) Hydrodynamic size distributions and (B) zeta potential values of CNC and CNC/5FU.

Table 1
Zeta potential and hydrodynamic particle size of the synthesized sample suspensions after four weeks of storage.

Sample	As-prepared	1 week	2 weeks	3 weeks	4 weeks
Zeta potential (mV) at pH 7.4					
CNC	−42.76 ± 1.4	−36.09 ± 1.6	−35.71 ± 2.6	−33.51 ± 1.4	−32.37 ± 0.8
CNC/5FU	−38.10 ± 1.7	−35.45 ± 2.2	−34.10 ± 0.9	−32.86 ± 1.5	−31.62 ± 1.1
Hydrodynamic particle size (nm) pH 7.4					
CNC	109.64 ± 2.8	148.11 ± 3.6	151.78 ± 2.9	155.16 ± 4.8	158.14 ± 2.6
CNC/5FU	119.25 ± 2.3	154.70 ± 4.1	158.58 ± 2.3	160.02 ± 3.5	161.36 ± 4.0

allow for spheroid formation. After 48-h, spheroid formation was confirmed by microscopic examination and 100 μL of each sample (0, 7.81, 15.62, 31.25, 62.53, 125, 250, and 500 μg/mL) was added into the wells, respectively. The plate was incubated at 37 °C, 5% CO_2 for 72-h. Then, spheroid inhibition was measured by a CellTiter-Glo 3D cell viability assay (#G9681, Promega) according to the manufacturer's instruction. Briefly, 100 μL of the CellTiter-Glo 3D reagent was added into each well, mixed vigorously for 5 min, and incubated at 37 °C for 30-min in the dark. The plate was then measured using the multimode microplate reader (Tecan). The dose-response graph was plotted by calculating the percent cell viability using Eq. (7):

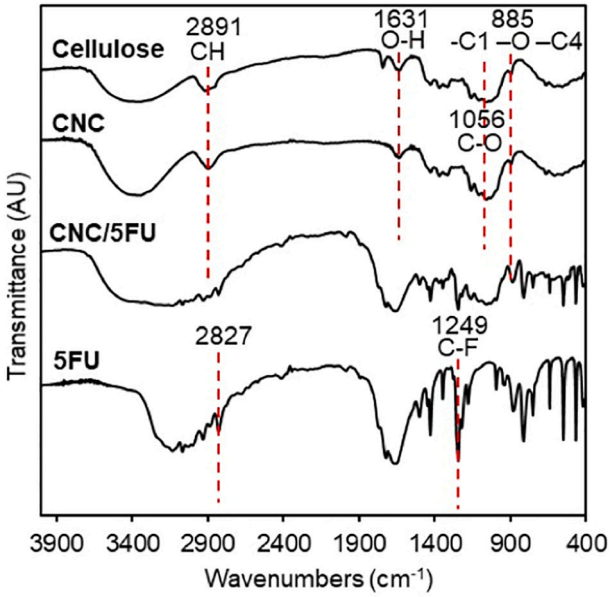

Fig. 6. FTIR results of cellulose, CNC, CNC/5FU, and 5FU.

$$\text{Cell viability}\ (\%) = \frac{\text{Relative luminescence unit (RLU) of sample well (mean)}}{\text{Relative luminescence unit (RLU) of control well (mean)}} \times 100 \quad (7)$$

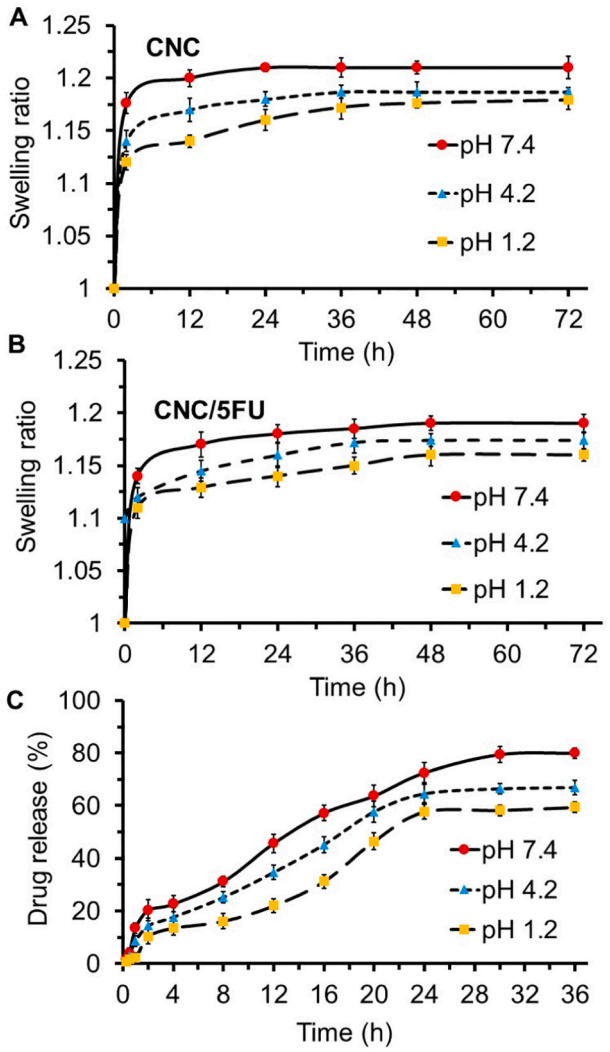

Fig. 7. Swelling kinetics of (A) CNC and (B) CNC/5FU initiated from the wet state in a pH 1.2, 4.2, and 7.4 medium. (C) Drug release performance from CNC/5FU in a pH 1.2, 4.2, and 7.4 medium.

Table 2
The calculated IC_{50} values for CNC, CNC/5FU, and 5FU on CCD-112, HCT116, and HT-29 cell lines.

IC_{50} value (μg/ml)	Normal cell	Cancer cells			
	CCD-112	HCT116		HT-29	
Culture model	2D	2D	3D	2D	3D
CNC	>500	>500	>500	>500	>500
CNC/5FU	84	71.7	94.6	213.8	>500
5FU	3.83	4.1	13.2	6.1	12.8

The inhibitory concentration causing 50% growth inhibition (IC_{50}) was determined through an online calculator (https://www.aatbio.com/tools/ic50-calculator) as previously described [29].

2.8. Tumor-on-chip experiment

Tumor spheroids were generated as described above, harvested and injected along with a Matrigel matrix (#354234, Corning) into 3D Cell Culture Chips (Aim Biotech, Singapore) as described previously [28]. The Matrigel was left for 30-min for polymerization. Fibronectin (#610077, BD) was prepared at 5 μg/mL and used to coat both side channels for cell adhesion. Next, CCD112 colon fibroblast cells were prepared at 1×10^6 cells/mL and injected into both side channels. The chip was incubated at 37 °C, 5% CO_2 overnight for complete adherence. 100 μg/mL of CNC and CNC/5FU were prepared and injected into the side channels followed by a 72-h incubation. Changes of the spheroids were monitored every 24-h and images were captured using an inverted microscope (AE2000 Motic). The size of the spheroids was measured using Motic Images Plus 3.0 Digital Camera software.

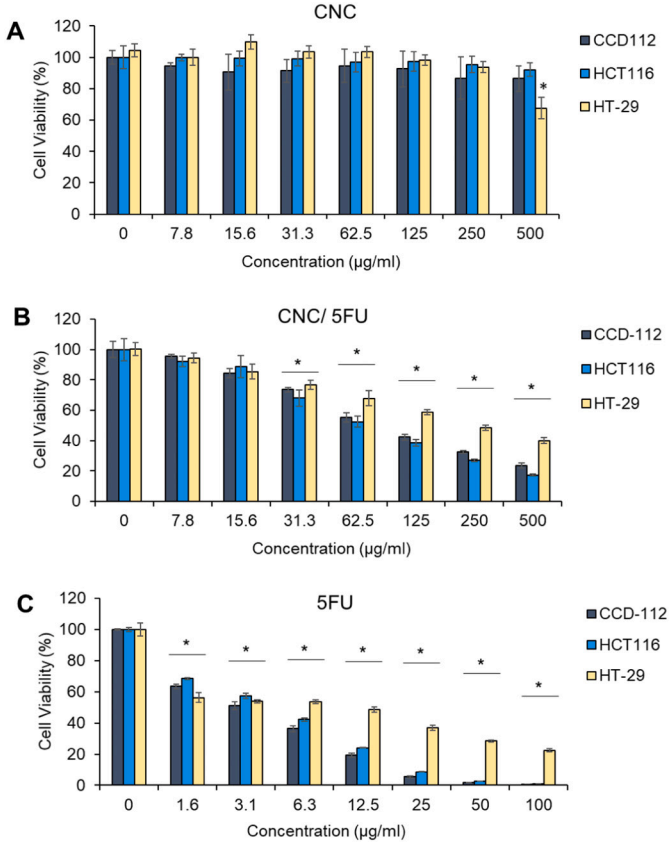

Fig. 8. Anticancer activity of (A) CNC, (B) CNC/5FU, and (C) 5FU against colorectal cell lines in 2D monolayer cultures. *$p < 0.05$.

2.9. Clonogenic assay

A clonogenic assay was performed on a 6-well plate following a modified protocol [30]. Cells ranging from a density from 100 to 100,000 cells per well were seeded onto the plate. After 24-h, cells in each plate were treated with five different concentrations (0, 31.3, 62.5, 125, 250, and 500 μg/mL) of CNC/5FU. After 72-h of incubation at 37 °C in a 95% air and 5% CO_2 incubator, medium containing CNC/5FU was removed and the cells and were cultured in fresh medium for an additional 10 days for adequate colony formation. At the end of incubation, cell colonies were stained with 0.25% *w/v* crystal violet (#C6158, Sigma-Aldrich) in 95% ethanol. After air drying, the images of the plates were captured and colonies with more than 50 cells were quantified and counted using Image J software (NIH). Plating efficiency (PE) and surviving fractions (SF) were calculated following the Eqs. (8) and (9) below [28]:

$$\mathrm{PE}\ (\%) = \frac{\text{number of colonies formed under untreated conditions}}{\text{number of seeded cells}} \times 100 \tag{8}$$

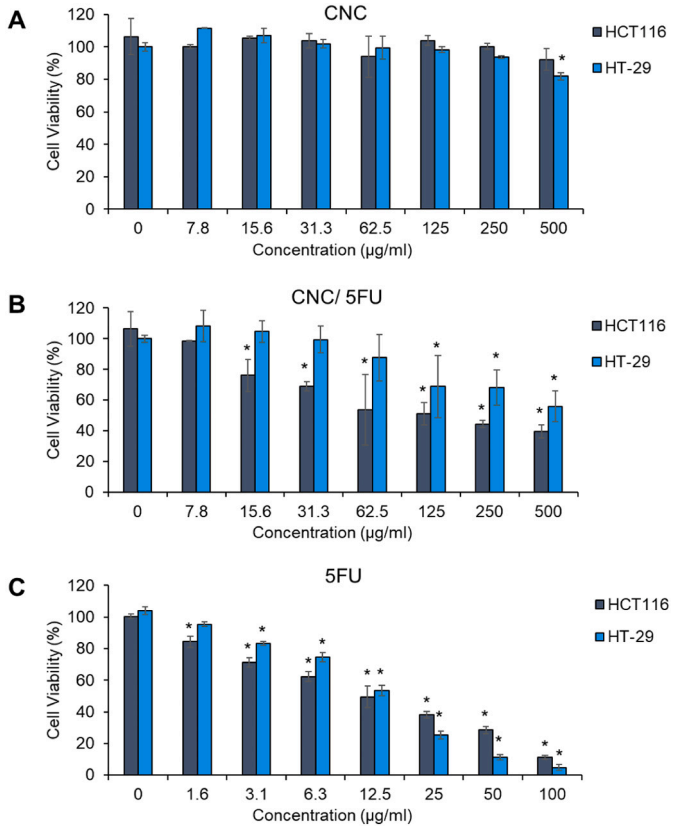

Fig. 9. Anticancer activity of (A) CNC, (B) CNC/5FU, and (C) 5FU against 3D tumor spheroids generated from HCT116 and HT-29 colorectal cancer cells. *p < 0.05.

$$\text{SF}\ (\%) = \frac{\text{number of colonies formed after treatment}}{\text{number of seeded cells x PE}} \times 100 \quad (9)$$

2.10. Apoptosis and necrosis assay

To evaluate whether CNC/5FU induced apoptosis and/or necrosis in the treated cells, Annexin V apoptosis and necrosis assays (#JA1011, Promega) were performed according to the manufacturer's instruction. HCT116 and HT-29 colorectal cancer cell lines were treated with 100 and 200 μg/mL CNC/5FU, respectively, for 72 h and the apoptosis/necrosis activity was measured using a multimode microplate reader (Tecan). The apoptotic activity was measured from the luminescence signals while necrotic activity was measured from the fluorescence signals ($485nm_{Ex}/530nm_{Em}$). The apoptotic and necrotic activity were compared to untreated controls and the positive control using 1 μM Bortezomib. The percent activity shown by the CNC/5FU was calculated following the Eq. (10) below:

$$\text{Percent activity}\ (\%) = \frac{\text{RLU/RFU of treated samples} - \text{RLU/RFU of untreated samples}}{\text{RLU/RFU of untreated samples}} \times 100 \quad (10)$$

2.11. Mitochondrial membrane potential assay

Cell vitality status was evaluated by examining the cellular mitochondrial function using the JC-1 mitochondrial membrane potential assay kit (#10009172, Cayman Chemical, MI, USA) following the manufacturer's instruction as previously described with slight modification [31]. HCT116 and HT-29 cells were treated with 100 and 200 μg/mL CNC/5FU, respectively, for 72 h and the mitochondrial behavior was assessed through JC-1 staining. In healthy cells, JC-1 forms complexes and form aggregates in red fluorescence meanwhile unhealthy cells exhibit green fluorescence. The health status of the cells was measured using a multimode microplate reader (Tecan) (excitation/emission - 535/595 nm for rhodamine and 485/535 nm for FITC). The ratio of fluorescence intensity of rhodamine (healthy cells) and FITC (unhealthy cells) was determined and plotted.

2.12. Statistical analysis

Independent experiments were performed three times and the data were expressed as the mean ± standard deviation for all triplicates within an individual experiment. Data were analyzed with a Student's *t*-test using SPSS version 26.0. $p < 0.05$ was considered statistically significant.

3. Results and discussion

Scheme 1A shows the procedures used in this study. Cellulose was isolated from rice straw waste and then it was treated with acid hydrolysis to obtain CNC. The rod-shaped CNC served as a 5FU carrier that subsequently caused the elimination of around 90% colorectal cancer cells in vitro. Scheme 1B shows the possible intermolecular chemical interactions between active functional groups in CNC/5FU. 5FU possibly had Van der Waals interactions with CNC [32]. During the drug loading process, the molecules of CNC potentially became nano-gels to increase the conjugation of 5FU with the CNC platform [33].

3.1. X-ray powder diffraction (XRD)

Fig. 1 shows the XRD results of the fabricated samples. Cellulose, CNC, and CNC/5FU had a similar XRD pattern, since the chemical treatments were sufficient and did not damage the main cellulose structure of the samples. The peaks approximately at $2\theta = 15.6°$, 22.4°, and 34.5° were attributed, respectively, to the 110, 200, and 004 planes in the normal cellulose-I structure. The main crystalline region was at 22.4° with a strong intensity, showing the high crystallinity of CNC. From Eq. (3), the crystallinity index of CNC and CNC/5FU was found to be 71.24% and 56.35%, respectively. The crystallite size is related to the crystallinity of the sample. From Eq. (4), 3.81 nm and 4.29 nm were calculated as the crystallite size of CNC and CNC/5FU with an interplanar distance of 3.72 nm and 5.64 nm, respectively. The acceptable crystallite size and crystallinity of the sample may show the effective alkali and acid hydrolysis treatments to degrade the amorphous region and liberate the crystalline region [34]. The XRD pattern of 5FU dis-

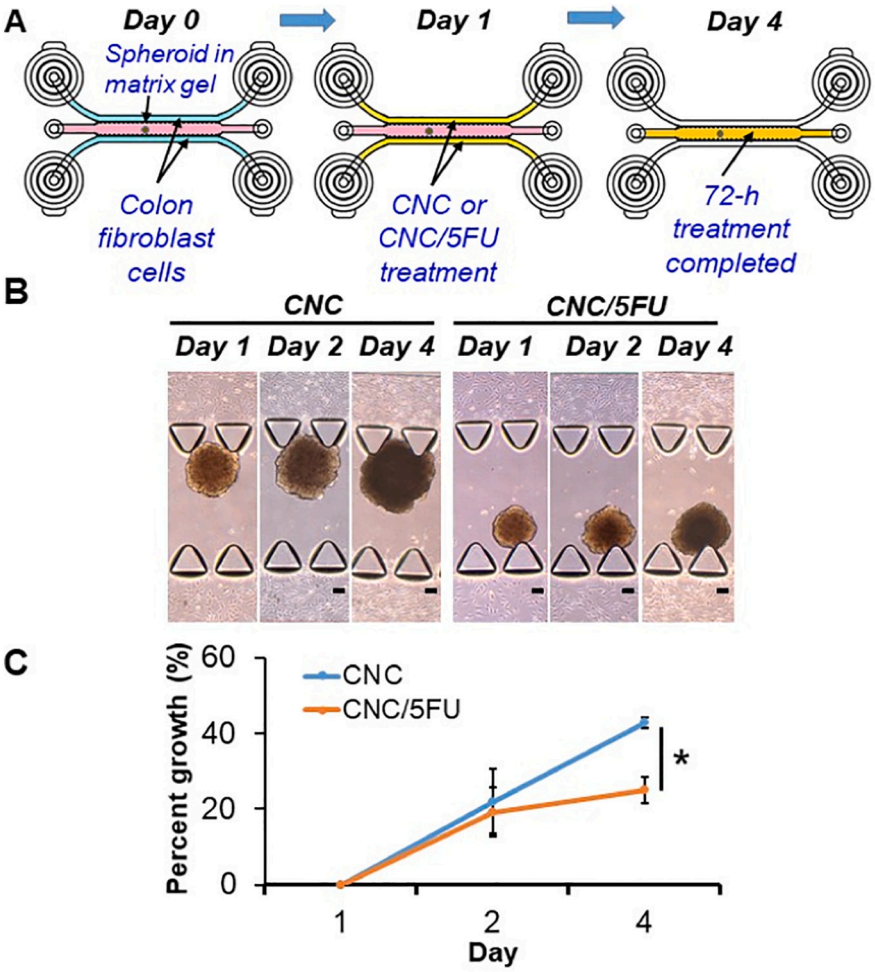

Fig. 10. Tumor spheroid-on-chip testing using CNC/5FU. (A) Schematic diagram showing the design of the spheroid-on-chip co-culture model and CNC/5FU treatment. (B) Microscopic examination and (C) spheroid size analysis of HCT116 spheroids treated with 100 μg/mL CNC and CNC/5FU. Scale bar represents 100 μm. *$p < 0.05$.

played various peaks at 16.5°, 19.3°, 20.7°, 22.1°, 28.7°, 31.4°, 32.2°, 33.5°, and 59.4°. The presence of the drug decreased the intensity of the peaks in CNC/5FU. Therefore, the loaded-5FU did not change the main crystalline structure of CNC.

3.2. Transmission electron microscopy (TEM) and energy dispersive X-ray (EDX) analysis

The results from TEM analysis for CNC/5FU are shown in Fig. 2A-D. CNC/5FU showed a rod-like and nano dimensional structure with an average length and width of 69.53 ± 1.14 nm and 8.13 ± 0.72 nm, respectively. The aspect (length to width) ratio of CNC/5FU was estimated to be 8.55, similar to a different report [35]. The TEM images indicated a homogeneous dispersion of CNC as comprised of individual and organized cellulosic fibrils with good surface area. As observed during the sample preparation for TEM, a drop of the CNC/5FU suspension was unchanged on the glass slide, addressing its high colloidal stability in the aqueous solution [36]. The slight agglomeration in the CNC/5FU images was possibly due to water evaporation during sample preparation for TEM analysis and also the possible high density of hydroxyl groups on the surface of the cellulose chains to form strong hydrogen bonds in CNC. Moreover, freeze-drying could cause negligible agglomeration among the cellulose fibrils of CNC [37]. Noticeably, the elimination of frozen water during freeze-drying could cause the well-established nanodimension and the porous structure of polysaccharide nanocrystals. This was also found in a different study on microcrystalline cellulose [38]. As shown in the EDX results (Fig. 2E and F), the CNC sample comprised 82.48 and 18.52 wt% of carbon and oxygen, respectively. Further results showed that CNC/5FU contained 57.14, 26.45, 14.23, and 2.17 wt% of carbon, oxygen, fluorine (F), and Na, respectively. The EDX data, thus, showed the elements related to the 5FU-loaded CNC.

3.3. Atomic force microscopy (AFM)

AFM images of a dilute suspension of CNC/5FU are shown in Fig. 3A-D. Representative fibrils are indicated by white arrows in Fig. 3A. In Fig. 3B, CNC/5FU contains the rods in the nano dimension with an average length and width of 135.27 ± 3.8 nm and 12.45 ± 2.6 nm, which is in agreement with the TEM results. Representative AFM morphology indicated isolated and individual CNCs [39]. As seen in Fig. 3C, the bright and dark regions represent the crystalline and the amorphous regions, respectively [40], showing that CNC/5FU possessed acceptable crystalline regions. The aggregation and stacking of CNC onto each other could cause a height higher than 100 nm, and the inter-hydrogen bonding binds the cellulose to each other after the drying procedure [41].

3.4. Thermal stability analysis

Fig. 4 shows TGA and DTGA results of CNC, CNC/5FU, and 5FU in which they indicated the major thermal degradation at 308.58 °C,

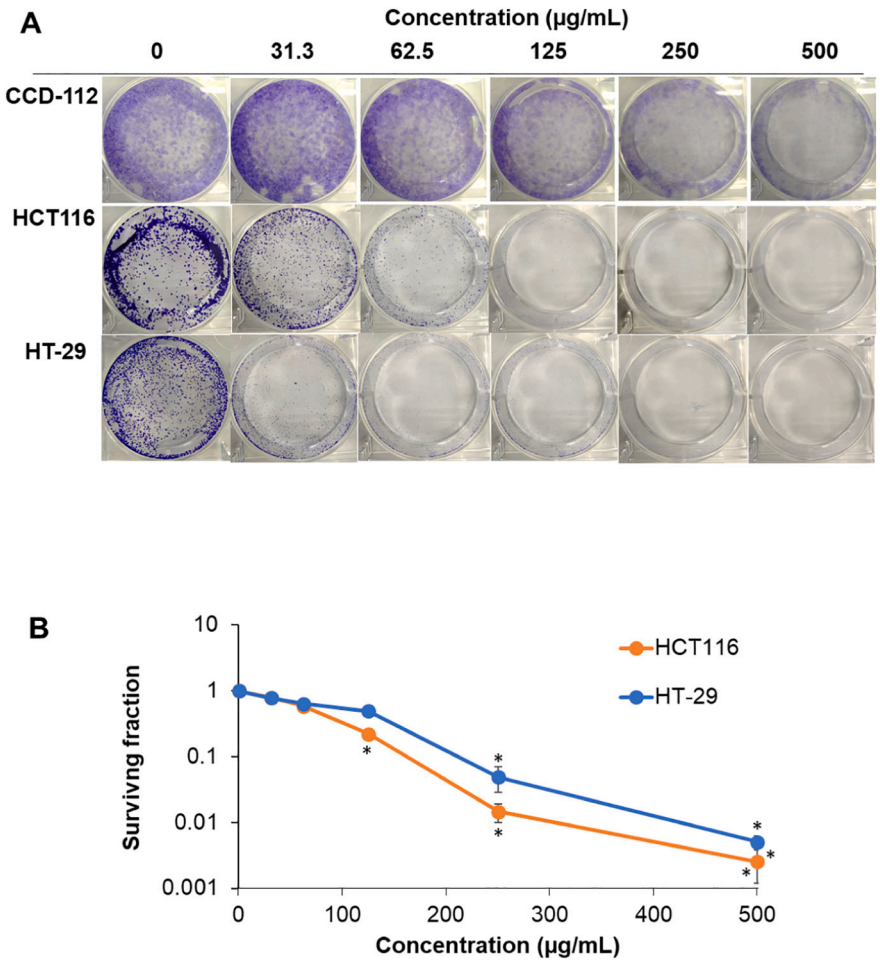

Fig. 11. Clonogenic assay by CNC/5FU on colorectal cell lines. (A) Images from colony-formation assays of the colorectal cell lines following a 0, 31.3, 62.5, 125, 250, and 500 μg/mL treatment of CNC/5FU; (B) The survival curve of HCT116 and HT-29 colorectal cancer cells treated with various concentrations of CNC/5FU. *$p < 0.05$.

332.53 °C and, 284.60 °C with the final residue of 12.07, 6.72, and 0.91 wt%, respectively. In the polysaccharide samples, this thermal degradation could be attributed to carbonyl and carboxyl groups triggering the reduction of the chain size and rapturing the bonds of the CNC [42]. 5FU alone indicated an increase in thermal stability after its loading onto the CNC carrier. TGA and DTGA analysis showed that the fabricated polysaccharide samples possessed acceptable thermal stability.

3.5. Dynamic light scattering (DLS) analysis

Fig. 5A and B shows the zeta potential and hydrodynamic size of the fabricated polysaccharide samples, respectively. The suspensions of CNC and CNC/5FU showed high negative zeta potentials of -42.76 ± 1.4 and -38.10 ± 1.7 mV, and a hydrodynamic size of 109.64 ± 2.8 and 119.25 ± 2.3 nm, respectively. Adding the drug onto CNC slightly decreased and increased the zeta potential value and the hydrodynamic size for CNC/5FU, respectively. Therefore, CNC with an acceptable negative zeta potential and nano-dimensional scale could be considered as a suitable 5FU carrier in cancer therapy. The small nanosize and narrow size distribution of CNC could be attributed to the suitable fabrication method used and the optimal ratio of the applied chemicals [43]. It has been stated that a narrow particle size distribution can lead to higher drug-loading efficiency [43]. In addition, it was stated that chemotherapeutic formulations with sizes below 150 nm [44–46] or 200 nm [47] show appropriate antitumor effects [48], which was seen in the CNC/5FU formulation here.

Table 1 shows the hydrodynamic size and zeta potential values of CNC and CNC/5FU after storage for 1, 2, 3, and 4 weeks in a PBS solution with pH 7.4. The CNC suspension showed similar colloidal stability with CNC/5FU after 4 weeks of storage. During the storage, the stability of the samples was marginally reduced, potentially due to the minor particle agglomeration. CNC and CNC/5FU indicated zeta potential values of -32.37 ± 0.8 and -31.62 ± 1.1 mV, respectively, after 4 weeks of storage, similar to a different study [49]. Particle sizes of the nanofluid samples at different storage times were obtained from DLS measurements (Table 1). A slight increase in the average particle size after the prolonged storage could be related to minor agglomeration in the nanocellulose; whereas there was no major agglomeration visually noticed on the sample suspension even after 4 weeks of storage. It could be understood from the DLS analysis that both nanofluids of CNC and CNC/5FU exhibited high stability after 4 weeks of storage.

3.6. Fourier-transform infrared spectroscopy (FTIR)

FTIR results of cellulose, CNC, and CNC/5FU are shown in Fig. 6. The peak at 1524 cm^{-1} (aromatic skeletal vibrations) was possibly attributed to the presence of the pyranose ring skeletal C–O–C bonds of cellulose. The intensity of this peak decreased after each treatment and subsequently was eradicated in the spectra of CNC [50]. The peaks at 760 and 491 cm^{-1} might be attributed to the removal of silica (Si–O–Si stretching) [21]. In addition, the peaks at 3352, 2891, and 1100 cm^{-1} could demonstrate –OH groups, C—H stretching, and the cellulose structure, respectively. The minor peak at 887 cm^{-1} in the anomeric region (950–700 cm^{-1}) could address the glycosidic —C_1—O—C_4 deformation

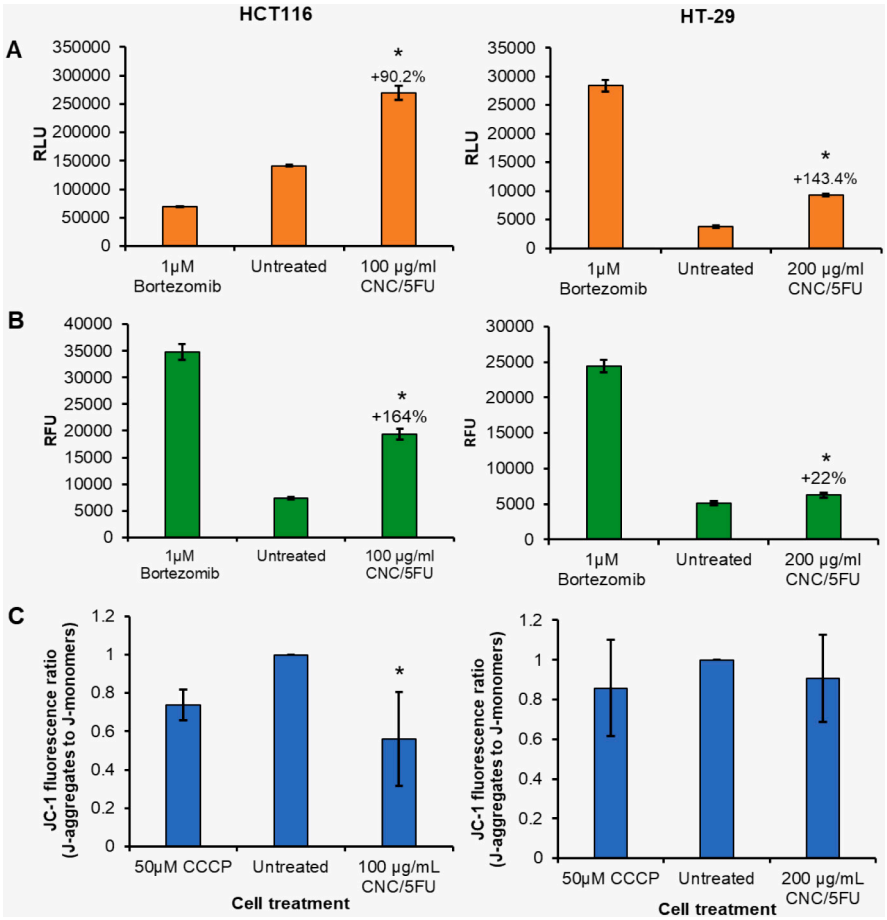

Fig. 12. Mechanistic studies of CNC/5FU killing on colorectal cancer cell lines. (A) Apoptosis assay; (B) Necrosis assay; and (C) Mitochondrial membrane potential assay. 1 μM bortezomib and 50 μM CCCP (carbonyl cyanide 3-chlorophenylhydrazone) were used as positive controls for the apoptosis/necrosis assay and mitochondrial JC-1 assays, respectively. RLU – relative luminescence units; RFU – relative fluorescence units. *$p < 0.05$.

properties of the β-glycosidic bond in cellulose and CNC. The FTIR spectrum of CNC/5FU was comparable to that of 5FU alone. The NH stretching groups in 5FU displayed a broadband at 2827–3300 cm^{-1}, whereas, it shifted to 2827–3500 cm^{-1} in the spectrum of CNC/5FU, because of the overlapping of the OH and NH bonds of 5FU. In summary, the FTIR results show the successful preparation of CNC to serve as the 5FU drug excipient.

3.7. Swelling analysis

Fig. 7A and B shows the swelling kinetics of CNC and CNC/5FU. Both samples in solutions at different pHs showed the main swelling ratio in the first 2-h. With increasing time and pH value, the increased swelling showed that CNC had a maximum swelling ratio of 1.179 ± 0.009, 1.187 ± 0.006, and 1.217 ± 0.011 in the media at pH 1.2, 4.2, and 7.4, respectively, after 72-h. Similarly, CNC/5FU indicated the highest swelling ratio of 1.19 ± 0.009 in media at pH 7.4. The CNC and CNC/5FU samples approximately showed their equilibrium state after 24-h. The above swelling results indicate the pH sensitivity of the fabricated polysaccharide samples.

3.8. Drug encapsulation efficiency (EE)% and loading capacity (LC)%

Based on Eq. (1), the LC was found to be 25.80 ± 1.27% and it was estimated that CNC/5FU approximately contained 26 and 74 wt% of the drug model and carrier, respectively. The EE was determined to be 83.50 ± 1.52%, according to Eq. (2). During the 5FU loading process, the CNC molecules in the aqueous solution possibly changed from chains to nano-gels to improve the conjugation between the dug and CNC [51]. Furthermore, 5FU is a heterocyclic aromatic organic compound with a low molecular weight, which can be diffused over the swollen CNC in the aqueous solution [52]. The acceptable LC and EE values imply that CNC/5FU can possibly decrease the 5FU administration dosage for improved cancer treatment.

3.9. In vitro drug release studies

Fig. 7C indicates the comparative drug release performance from CNC/5FU. The time taken for releasing about 13.51 ± 2.80%, 17.68 ± 3.50%, and 22.68 ± 3.00% of the drug was 4-h in the release media at pH 1.2, 4.2, and 7.4, respectively. The sustained drug release increased over time and the highest release rates were 59.41 ± 2.21%, 66.95 ± 4.81% and 80.04 ± 3.16%, in the medium at pH 1.2, 4.2, and 7.4, respectively, after 36-h. In the releasing procedure, the loaded-5FU dissolved in the CNC/5FU complex and achieved equilibrium between the solution and CNC, then the released-drug outside of the complex was completely dissolved within the extracellular media [53]. The release mechanism might be associated with the swelling capacity, dissolution and diffusion rate, and the functional groups of CNC/5FU. The drug release showed a similar trend with the swelling ratio of the samples. 5FU release was lower in the simulated acidic fluid at pH 1.2 and 4.2 compared to that in the fluid at pH 7.4 [54]. This can be explained that CNC/5FU became smaller in the acidic media [55]. The swelling may lead to polymer relaxation to obtain a controlled drug release profile from CNC/5FU [53]. In summary, CNC/5FU presented a sustained and pH sensitive release behavior.

3.10. In vitro anticancer assays

Cytotoxic effects of CNC and CNC/5FU were assessed on CCD112 colon normal cells and colorectal cancer cells (HCT116 and HT-29). The anticancer drug 5FU was included as the positive control. Table 2 summarizes the anticancer activities of CNC, CNC/5FU, and 5FU against colon normal and cancer cells in both 2D monolayer and 3D spheroid models. No obvious cytotoxic effect was seen in the CNC-treated cells except for HT-29 cells at the highest test concentration of 500 μg/mL (Fig. 8A). This supports the non-toxic property of CNC to act as a potential drug nanocarrier. A separate study found that the shorter size (<50 nm) of CNC showed a high toxicity of almost 50% against murine embryo fibroblasts (NIH3T3) and colon adenocarcinoma cells [56]. In comparison, the larger size of CNC (1174 nm) at a concentration above 250 μg/mL indicated higher toxicity because of its ability to be formed as a gel in an aqueous solution [56]. In the 2D monolayer models, CNC/5FU showed dose-dependent cytotoxicity in HCT116 (IC_{50}-71.7 μg/mL) followed by CCD112 (IC_{50}-84 μg/mL) and HT-29 (IC_{50}-213.8 μg/mL) (Fig. 8B). The cytotoxicity of CNC/5FU towards CCD112 colon normal cells was observed and this must be taken into consideration for further nanocarrier modification and development. The different level of cytotoxicity shown by CNC/5FU suggests that the activity is cell-specific and it may be accompanied by various mechanisms and/or resistance mechanisms [57].

In 3D spheroid models, the reduced anticancer action of CNC/5FU (shown by increased IC_{50} values) was seen in all colon cancer cell lines (Table 2). This could be due to the different tissue architecture of the spheroid, which might partly block the penetration of the CNC/5FU as compared to the 2D monolayer model [58]. Similar to the findings from 2D monolayer models, CNC was generally not reactive to the tested cells except for HT-29 (~19% killing) at 500 μg/mL (Fig. 9A). The use of a 3D spheroid model has been known to more accurately represent the in vivo tumor and recapitulate the in vivo state, hence, resulting in a more translatable anticancer outcome or more predictable treatment efficiency in pre-clinical models [59]. As shown in Fig. 9B, our findings show that CNC/5FU is more potent against HCT116 (IC_{50}-94.6 μg/mL) than HT-29 (IC_{50}->500 μg/mL) cells (Table 2). This variation could be due to the different characteristics of the tested cells including both phenotypic and genotypic profiles. Further experiments need to be conducted to investigate the target specificity of CNC/5FU as the current findings suggest that the anticancer action may be cell-specific (more potent against HCT116 than HT-29 cells).

To further assess the anticancer action of CNC/5FU on HCT116 spheroids, a microfluidic chip-based co-culture model was generated. A HCT116 spheroid was grown in the middle channel of the chip in the presence of an extracellular matrix (ECM) gel flanked by both side channels seeded with CCD112 colon fibroblasts followed by a 72-h treatment of 100 μg/mL of CNC/5FU and CNC (Fig. 10A). The growth of the spheroid based on the size differences was measured and compared over the 72-h treatment (Fig. 10B). From the microscopic examination, CNC/5FU significantly inhibited the growth of the spheroid compared to the CNC-treated spheroid. Both CNC and CNC/5FU did not affect the growth of the seeded CCD112 colon fibroblasts as an increasing number of CCD112 cells was observed. This observation is contradictory with the anticancer assay using the 2D monolayer as shown by Fig. 8B. This variation could be due to the higher tolerance of CCD112 cells towards CNC/5FU when seeded at a higher density, this further supports the safety of using CNC/5FU as the nanodrug. Fig. 10C shows that CNC/5FU significantly reduced the growth rate of the spheroid at about 20% compared to the CNC-treated spheroid.

3.11. Clonogenic survival assay

The clonogenic assay showed the effect of CNC/5FU on the colony-forming capacity of various exponentially growing cells (Fig. 11). Concentration-dependent growth inhibition of CNC/5FU was observed in crystal violet-stained cells (Fig. 11A), which is consistent with the previous findings in Fig. 9B. Inhibition of CNC/5FU on colony formation was reduced in CCD112 cells compared to other colorectal cancer cell lines at the same concentrations. After treatment with different concentrations (31.3, 62.5, 125, 250, and 500 μg/mL), the surviving fraction of all the tested colon cancer cells declined (Fig. 11B), as evidenced by the reduction in the number of colonies formed. CCD112 data was not included in the survival curve as colonies could not be enumerated from the plates. The fibroblastic cells formed spindle-shaped cells spread out on the well rather than forming colonies. Fig. 11B indicates that CNC/5FU significantly inhibited the colony formation capabilities of HCT116 and HT-29 cells at concentrations above 125 and 250 μg/mL, respectively. These findings corroborated well with the monolayer cell proliferation study as shown in Fig. 8B. Both short-term cell proliferation assays (72-h) and long-term colony-formation assays (10 days) support the cytotoxic effects of CNC/5FU towards colorectal cancer cells, thereby representing a potential anticancer drug worthy of further investigation.

3.12. Mechanistic studies of CNC/5FU killing

To investigate the anticancer mechanism of CNC/5FU, the apoptotic and necrotic activities of the cells treated with CNC/5FU compared to the untreated cells were determined. Fig. 12A shows a 90.2% and 143.4% increase in apoptotic activity based on the luminescence signals in CNC/5FU-treated HCT116 and HT-29 cells, respectively. Bortezomib was used as the positive control to induce apoptosis and necrosis in both cells, however, it failed to induce the apoptosis in HCT116 cells. Surprisingly, high necrotic activity (an increase of 164%) was seen in HCT116 cells treated with CNC/5FU while only a modest increase of necrosis (22%) was seen in CNC/5FU-treated HT-29 cells (Fig. 12B). Taken together, this finding suggests that CNC/5FU kills the cancer cells by mainly inducing apoptosis. This is consistent with our previous work [28] that the 5FU loaded magnetic cellulose bionanocomposites killed HCT116 and HT-29 cells by inducing apoptosis from the observed increased caspase activity.

A mitochondrial membrane potential assay was then performed to determine if the CNC/5FU could inhibit cancer cells by inducing mitochondrial damage. In this assay, a cytofluorimetric cationic dye, JC-1 forms a complex known as J-aggregates with red fluorescence (rhodamine) in healthy cells, while JC-1 remains in monomeric form and exhibits green FITC in unhealthy cells. As shown in Fig. 12C, the CNC/5FU-treated cells displayed a lower ratio of J-aggregates to J-monomers, indicating 0.56 and 0.91 for HCT116 and HT-29, respectively. This suggests that CNC/5FU could induce mitochondrial damage which then leads to cancer cell death; this effect was more apparent in the treated HCT116 compared to HT-29 cells. Similar to apoptosis induction, mitochondrial damage induction was also observed in a treatment with 5FU-loaded magnetic cellulose bionanocomposites from our recent work [28].

4. Conclusion

This study aimed to synthesize a nanodrug formulation of CNC/5FU for in vitro colorectal cancer treatment. CNC was successfully extracted from rice straw cellulose by alkali and acid hydrolysis treatments. According to XRD and FTIR results, the series of treatments on the cellulose mostly removed hemicellulose and lignin to liberate crystallized CNC. TEM and AFM images indicated the rod-shaped nanostructures of CNC/5FU with low agglomeration. The fabricated polysaccharide samples exhibited high thermal and colloidal stability. In vitro anticancer assays demonstrated that CNC/5FU was potent against HCT116 and HT-29 colorectal cancer cells, and insignificant cytotoxicity was seen in CCD112 colon normal cells. CNC/5FU killed the cancer cells by inducing cell apoptosis and mitochondrial membrane damage. This research suggests that 5FU-loaded CNC could be a promising nanodrug system for

future cancer treatment. Future in vivo studies on CNC/5FU will further elucidate their promise.

CRediT authorship contribution statement

Mostafa Yusefi: Writing - original draft, Conceptualization, Methodology, Investigation, Formal analysis, Data curation, Validation, Resources, Data curation.

Michiele Lee-Kiun Soon: Formal analysis, Writing - review & editing, Investigation.

Sin-Yeang Teow: Resources, Methodology, Writing - review & editing, Data curation, Investigation, Formal analysis, Funding acquisition.

Elaine Irene Monchouguy: Formal analysis, Investigation.

Bibi Noorheen Haleema Mooneerah: Formal analysis, Visualization.

Zahra Izadiyan: Writing - review & editing.

Hossein Jahangirian: Validation, Review & editing.

Roshanak Rafiee-Moghaddam: Validation.

Thomas J. Webster: Writing - review & editing.

Kamyar Shameli: Funding acquisition, Methodology, Conceptualization, Investigation, Resources, Formal analysis, Data curation, Supervision, Writing - review & editing.

Declaration of competing interest

The authors declare no conflict of interest.

Acknowledgments

This research was funded by a Takasago Thermal Engineering Co. Ltd. grant (R.K130000.7343.4B422) from the research management center (RMC) of Universiti Teknologi Malaysia (UTM) and Malaysia-Japan International Institute of Technology (MJIIT). Special thanks to the School of Medical and Life Sciences, Sunway University cell culture facilities for the anticancer assays which was partly supported by Individual Research Grant 2021 (GRTIN-IRG-17-2021).

References

[1] M. Baroud, E. Lepeltier, S. Thepot, Y. El-Makhour, O. Duval, The evolution of nucleosidic analogues: self-assembly of prodrugs into nanoparticles for cancer drug delivery, Nanoscale Adv. 3 (8) (2021) 2157–2179, https://doi.org/10.1039/D0NA01084G.

[2] J. Shi, P.W. Kantoff, R. Wooster, O.C. Farokhzad, Cancer nanomedicine: progress, challenges and opportunities, Nat.Rev. Cancer 17 (1) (2017) 20–37, https://doi.org/10.1038/nrc.2016.108.

[3] P. Rai, S. Mehrotra, S. Priya, E. Gnansounou, S.K. Sharma, Recent advances in the sustainable design and applications of biodegradable polymers, Bioresour. Technol. (2021), 124739, https://doi.org/10.1016/j.biortech.2021.124739.

[4] M.Carmen Chifiriuc, A.Mihai Grumezescu, V. Grumezescu, E. Bezirtzoglou, V. Lazar, A. Bolocan, Biomedical applications of natural polymers for drug delivery, Curr. Org. Chem. 18 (2) (2014) 152–164, https://doi.org/10.2174/1385272818021401291045 25.

[5] P. Mali, A.P. Sherje, Cellulose nanocrystals: fundamentals and biomedical applications, Carbohydr. Polym. (2021), 118668, https://doi.org/10.1016/j.carbpol.2021.118668.

[6] S. Sarkar, N. Levi-Polyachenko, Conjugated polymer nano-systems for hyperthermia, imaging and drug delivery, Adv.Drug Deliv. Rev. 163 (2020) 40–64, https://doi.org/10.1016/j.addr.2020.01.002.

[7] H. Jahangirian, B. Saleh, K. Kalantari, R. Rafiee-Moghaddam, B. Nikpey, S. Jahangirian, T.J. Webster, Enzymatic synthesis of ricinoleyl hydroxamic acid based on commercial castor oil, cytotoxicity properties and application as a new anticancer agent, Int. J. Nanomedicine 15 (2020) 2935, https://doi.org/10.2147/IJN.S223796.

[8] S. Nasri, B. Ebrahimi-Hosseinzadeh, M. Rahaie, A. Hatamian-Zarmi, R. Sahraeian, Thymoquinone-loaded ethosome with breast cancer potential: optimization, in vitro and biological assessment, J. Nanostruct. Chem. 10 (1) (2020) 19–31, https://doi.org/10.1007/s40097-019-00325-w.

[9] C.-E. Iurciuc-Tincu, M.S. Cretan, V. Purcar, M. Popa, O.M. Daraba, L.I. Atanase, L. Ochiuz, Drug delivery system based on pH-sensitive biocompatible poly (2-vinyl pyridine)-b-poly (ethylene oxide) nanomicelles loaded with curcumin and 5-fluorouracil, Polymers 12 (7) (2020) 1450, https://doi.org/10.3390/polym12071450.

[10] T. He, W. Wang, B. Chen, J. Wang, Q. Liang, B. Chen, 5-Fluorouracil monodispersed chitosan microspheres: microfluidic chip fabrication with crosslinking, characterization, drug release and anticancer activity, Carbohydr. Polym. 236 (2020), 116094, https://doi.org/10.1016/j.carbpol.2020.116094.

[11] R. Parhi, Drug delivery applications of chitin and chitosan: a review, Environ. Chem. Lett. 18 (3) (2020) 577–594, https://doi.org/10.1007/s10311-020-00963-5.

[12] F. Wang, Q. Zhang, K. Huang, J. Li, K. Wang, K. Zhang, X. Tang, Preparation and characterization of carboxymethyl cellulose containing quaternized chitosan for potential drug carrier, Int.J. Biol. 154 (2020) 1392–1399, https://doi.org/10.1016/j.ijbiomac.2019.11.019.

[13] D. Mohan, N.F. Khairullah, Y.P. How, M.S. Sajab, H. Kaco, 3D printed laminated CaCO3-nanocellulose films as controlled-release 5-fluorouracil, Polymers 12 (4) (2020) 986, https://doi.org/10.3390/polym12040986.

[14] A. Karimian, H. Parsian, M. Majidinia, M. Rahimi, S.M. Mir, H.S. Kafil, V. Shafiei-Irannejad, M. Kheyrollah, H. Ostadi, B. Yousefi, Nanocrystalline cellulose: preparation, physicochemical properties, and applications in drug delivery systems, Int.J. Biol. 133 (2019) 850–859, https://doi.org/10.1016/j.ijbiomac.2019.04.117.

[15] Y. Gao, X. Guo, Y. Liu, Z. Fang, M. Zhang, R. Zhang, L. You, T. Li, R.H. Liu, A full utilization of rice husk to evaluate phytochemical bioactivities and prepare cellulose nanocrystals, Sci. Rep. 8 (1) (2018) 1–8, https://doi.org/10.1038/s41598-018-27635-3.

[16] N. Lin, A. Dufresne, Nanocellulose in biomedicine: current status and future prospect, Eur.Polym. J. 59 (2014) 302–325, https://doi.org/10.1016/j.eurpolymj.2014.07.025.

[17] C.J. Wijaya, S. Ismadji, S. Gunawan, A review of lignocellulosic-derived nanoparticles for drug delivery applications: lignin nanoparticles, xylan nanoparticles, and cellulose nanocrystals, Molecules 26 (3) (2021) 676, https://doi.org/10.3390/molecules26030676.

[18] W. Long, H. Ouyang, C. Zhou, W. Wan, S. Yu, K. Qian, M. Liu, X. Zhang, Y. Feng, Y. Wei, Simultaneous surface functionalization and drug loading: a novel method for fabrication of cellulose nanocrystals-based pH responsive drug delivery system, Int.J. Biol. (2021), https://doi.org/10.1016/j.ijbiomac.2021.05.193.

[19] L.E. Low, L.T.-H. Tan, B.-H. Goh, B.T. Tey, B.H. Ong, S.Y. Tang, Magnetic cellulose nanocrystal stabilized Pickering emulsions for enhanced bioactive release and human colon cancer therapy, Int.J. Biol. 127 (2019) 76–84, https://doi.org/10.1016/j.ijbiomac.2019.01.037.

[20] G.M.N. Ntoutoume, R. Granet, J.P. Mbakidi, F. Brégier, D.Y. Léger, C. Fidanzi-Dugas, V. Lequart, N. Joly, B. Liagre, V. Chaleix, Development of curcumin–cyclodextrin/cellulose nanocrystals complexes: new anticancer drug delivery systems, <sb:contribution><sb:title>Bioorg. Med. Chem.</sb:title></sb:contribution><sb:host><sb:issue><sb:series><sb:title>Lett.</sb:title></sb:series></sb:issue></sb:host> 26 (3) (2016) 941–945, https://doi.org/10.1016/j.bmcl.2015.12.060.

[21] M. Yusefi, K. Shameli, H. Jahangirian, S.-Y. Teow, H. Umakoshi, B. Saleh, R. Rafiee-Moghaddam, T.J. Webster, The potential anticancer activity of 5-fluorouracil loaded in cellulose fibers Isolated from rice straw, Int.J. Nanomedicine 15 (2020) 5417–5432, https://doi.org/10.2147/IJN.S250047.

[22] H.M. El-Zeiny, M.R. Abukhadra, O.M. Sayed, A.H. Osman, S.A. Ahmed, Insight into novel β-cyclodextrin-grafted-poly (N-vinylcaprolactam) nanogel structures as advanced carriers for 5-fluorouracil: equilibrium behavior and pharmacokinetic modeling, Colloids Surf.A Physicochem. Eng. Asp. 586 (2020), 124197, https://doi.org/10.1016/j.colsurfa.2019.124197.

[23] M. Yusefi, K. Shameli, Z. Hedayatnasab, S.-Y. Teow, U.N. Ismail, C.A. Azlan, R. R. Ali, Green synthesis of Fe 3 O 4 nanoparticles for hyperthermia, magnetic resonance imaging and 5-fluorouracil carrier in potential colorectal cancer treatment, Res.Chem. Intermed. (2021) 1–20, https://doi.org/10.1007/s11164-020-04388-1.

[24] J.K. Ogunjobi, O.M. Balogun, Isolation, modification and characterisation of cellulose from wild Dioscorea bulbifera, Sci.Rep. 11 (1) (2021) 1–10, https://doi.org/10.1038/s41598-020-78533-6.

[25] C. Trilokesh, K.B. Uppuluri, Isolation and characterization of cellulose nanocrystals from jackfruit peel, Sci.Rep. 9 (1) (2019) 1–8, https://doi.org/10.1038/s41598-019-53412-x.

[26] M. Yusefi, H.-Y. Chan, S.-Y. Teow, P. Kia, M. Lee-Kiun Soon, N.A.B.C. Sidik, K. Shameli, 5-Fluorouracil encapsulated chitosan-cellulose fiber bionanocomposites: synthesis,characterization and in vitro analysis towards colorectal cancer cells, Nanomaterials 11 (7) (2021) 1691, https://doi.org/10.3390/nano11071691.

[27] M. Yusefi, K. Shameli, R.R. Ali, S.-W. Pang, S.-Y. Teow, Evaluating anticancer activity of plant-mediated synthesized iron oxide nanoparticles using Punica granatum fruit peel extract, J. Mol. Struct. 1204 (2020), 127539, https://doi.org/10.1016/j.molstruc.2019.127539.

[28] M. Yusefi, M.S. Lee-Kiun, K. Shameli, S.-Y. Teow, R.R. Ali, K.-K. Siew, H.-Y. Chan, M.M.-T. Wong, W.-L. Lim, K. Kuča, 5-Fluorouracil loaded magnetic cellulose bionanocomposites for potential colorectal cancer treatment, Carbohydr. Polym. (2021), 118523, https://doi.org/10.1016/j.carbpol.2021.118523.

[29] Z. Izadiyan, K. Shameli, S.-Y. Teow, M. Yusefi, P. Kia, E. Rasouli, M.A. Tareq, Anticancer activity of 5-fluorouracil-loaded nanoemulsions containing Fe3O4/Au core-shell nanoparticles, J. Mol. Struct. (2021), 131075, https://doi.org/10.1016/j.molstruc.2021.131075.

[30] F. Meng, D. Bhupathi, C.P. Hart, An efficient clonogenic assay for cytotoxic drug screening, AACR (2010), https://doi.org/10.1158/1538-7445.AM10-5497.

[31] K.X. Lee, K. Shameli, S.E. Mohamad, Y.P. Yew, E.D. Mohamed Isa, H.-Y. Yap, W. L. Lim, S.-Y. Teow, Bio-mediated synthesis and characterisation of silver

nanocarrier, and its potent anticancer action, Nanomaterials 9 (10) (2019) 1423, https://doi.org/10.3390/nano9101423.
[32] T. Doane, C. Burda, Nanoparticle mediated non-covalent drug delivery, Adv.Drug Deliv. Rev. 65 (5) (2013) 607–621.
[33] K. Zhu, T. Ye, J. Liu, Z. Peng, S. Xu, J. Lei, H. Deng, B. Li, Nanogels fabricated by lysozyme and sodium carboxymethyl cellulose for 5-fluorouracil controlled release, Int.J. Pharm. 441 (1–2) (2013) 721–727, https://doi.org/10.1016/j.ijpharm.2012.10.022.
[34] M. Thakur, A. Sharma, V. Ahlawat, M. Bhattacharya, S. Goswami, Process optimization for the production of cellulose nanocrystals from rice straw derived α-cellulose, Mater.Sci. Technol. 3 (2020) 328–334, https://doi.org/10.1016/j.mset.2019.12.005.
[35] P. Li, Z. Yang, Y. Wang, Z. Peng, S. Li, L. Kong, Q. Wang, Microencapsulation of coupled folate and chitosan nanoparticles for targeted delivery of combination drugs to colon, J. Microencapsul. 32 (1) (2015) 40–45, https://doi.org/10.3109/02652048.2014.944947.
[36] K. Mondal, S. Sakurai, Y. Okahisa, V.V. Goud, V. Katiyar, Effect of cellulose nanocrystals derived from Dunaliella tertiolecta marine green algae residue on crystallization behaviour of poly (lactic acid), Carbohydr.Polym. 261 (2021), 117881, https://doi.org/10.1016/j.carbpol.2021.117881.
[37] J. Nemoto, T. Saito, A. Isogai, Simple freeze-drying procedure for producing nanocellulose aerogel-containing, high-performance air filters, ACS ApplMater. Interfaces 7 (35) (2015) 19809–19815, https://doi.org/10.1021/acsami.5b05841.
[38] E. Qua, P. Hornsby, H. Sharma, G. Lyons, Preparation and characterisation of cellulose nanofibres, J. Mater. Sci. 46 (18) (2011) 6029–6045, https://doi.org/10.1007/s10853-011-5565-x.
[39] N. Li, H. Bian, J. Zhu, P.N. Ciesielski, X. Pan, Tailorable cellulose II nanocrystals (CNC II) prepared in mildly acidic lithium bromide trihydrate (MALBTH), Green Chem. 23 (7) (2021) 2778–2791, https://doi.org/10.1039/D1GC00145K.
[40] H. Onkarappa, G. Prakash, G. Pujar, C.Rajith Kumar, V.S. Betageri, Facile synthesis and characterization of nanocellulose from Zea mays husk, Polym. Compos. 41 (8) (2020) 3153–3159, https://doi.org/10.1002/pc.25606.
[41] M.S. Mohaiyiddin, O.H. Lin, W.T. Owi, C.H. Chan, C.H. Chia, S. Zakaria, H.M. Akil, Characterization of nanocellulose recovery from Elaeis guineensis frond for sustainable development, Clean Technol.Environ. Policy 18 (8) (2016) 2503–2512, https://doi.org/10.1007/s10098-016-1191-2.
[42] S.-C. Pech-Cohuo, G. Canche-Escamilla, A. Valadez-González, V.V.A. Fernández-Escamilla, J. Uribe-Calderon, Production and modification of cellulose nanocrystals from Agave tequilana weber waste and its effect on the melt rheology of PLA int, J. Polym. Sci. 2018 (2018), https://doi.org/10.1155/2018/3567901.
[43] M. Abyadeh, A.A.K. Zarchi, M.A. Faramarzi, A. Amani, Evaluation of factors affecting size and size distribution of chitosan-electrosprayed nanoparticles Avicenna, J. Med. Biotechnol. 9 (3) (2017) 126.
[44] M. Mozafari, A. Pardakhty, S. Azarmi, J. Jazayeri, A. Nokhodchi, A. Omri, Role of nanocarrier systems in cancer nanotherapy, J. Liposome Res. 19 (4) (2009) 310–321.
[45] P.Y. Aw-Yong, P.H. Gan, A.O. Sasmita, S.T. Mak, A. Ling, Nanoparticles as carriers of phytochemicals: recent applications against lung cancer, Int. J. Res. Biomed. Biotechnol. 7 (2018) 1–11.
[46] K. Greish, J. Fang, T. Inutsuka, A. Nagamitsu, H. Maeda, Macromolecular therapeutics, Clin. Pharmacokinet. 42 (13) (2003) 1089–1105, https://doi.org/10.2165/00003088-200342130-00002.
[47] H. Maeda, Toward a full understanding of the EPR effect in primary and metastatic tumors as well as issues related to its heterogeneity, Adv. Drug Deliv. Rev. 91 (2015) 3–6, https://doi.org/10.1016/j.addr.2015.01.002.
[48] M. Danaei, M. Dehghankhold, S. Ataei, F.Hasanzadeh Davarani, R. Javanmard, A. Dokhani, S. Khorasani, M. Mozafari, Impact of particle size and polydispersity index on the clinical applications of lipidic nanocarrier systems, Pharmaceutics 10 (2) (2018) 57, https://doi.org/10.3390/pharmaceutics10020057.
[49] S.N. Molnes, K.G. Paso, S. Strand, K. Syverud, The effects of pH, time and temperature on the stability and viscosity of cellulose nanocrystal (CNC) dispersions: implications for use in enhanced oil recovery, Cellulose 24 (10) (2017) 4479–4491, https://doi.org/10.1007/s10570-017-1437-0.
[50] Q. Chen, Z. Zong, X. Gao, Y. Zhao, J. Wang, Preparation and characterization of nanostarch-based green hard capsules reinforced by cellulose nanocrystals int, J. Biol. 167 (2021) 1241–1247, https://doi.org/10.1016/j.ijbiomac.2020.11.078.
[51] A. Rehman, S.M. Jafari, Q. Tong, T. Riaz, E. Assadpour, R.M. Aadil, S. Niazi, I. M. Khan, Q. Shehzad, A. Ali, Drug nanodelivery systems based on natural polysaccharides against different diseases, Adv. Colloid Interf. Sci. 102251 (2020), https://doi.org/10.1016/j.cis.2020.102251.
[52] M.H. Mohammed, F.H. Hanoon, Zinc oxide nanosheet as a promising route for carrier 5-fluorouracil anticancer drug in the presence metal impurities: insights from DFT calculations, Comput. Theor. Chem. 1194 (2021), 113079, https://doi.org/10.1016/j.comptc.2020.113079.
[53] B. Sun, M. Zhang, J. Shen, Z. He, P. Fatehi, Y. Ni, Applications of cellulose-based materials in sustained drug delivery systems, Curr. Med. Chem. 26 (14) (2019) 2485–2501, https://doi.org/10.2174/0929867324666170705143308.
[54] T.S. Anirudhan, J. Nima, P.L. Divya, Synthesis, characterization and in vitro cytotoxicity analysis of a novel cellulose based drug carrier for the controlled delivery of 5-fluorouracil, an anticancer drug, Appl. Surf. Sci. 355 (2015) 64–73, https://doi.org/10.1016/j.apsusc.2015.07.077.
[55] J. Bhandari, H. Mishra, P.K. Mishra, R. Wimmer, F.J. Ahmad, S. Talegaonkar, Cellulose nanofiber aerogel as a promising biomaterial for customized oral drug delivery, Int. J. Nanomedicine 12 (2017) 2021, https://doi.org/10.2147/IJN.S124318.
[56] Z. Hanif, F.R. Ahmed, S.W. Shin, Y.-K. Kim, S.H. Um, Size-and dose-dependent toxicity of cellulose nanocrystals (CNC) on human fibroblasts and colon adenocarcinoma, Colloids Surf.B: Biointerfaces 119 (2014) 162–165, https://doi.org/10.1016/j.colsurfb.2014.04.018.
[57] K.P. Mr, P.R. Iyer, Antiproliferative effects on tumor cells of the synthesized gold nanoparticles against Hep2 liver cancer cell line, EgyptLiver J 10 (1) (2020) 1–12, https://doi.org/10.1186/s43066-020-0017-4.
[58] M. Vinci, S. Gowan, F. Boxall, L. Patterson, M. Zimmermann, C. Lomas, M. Mendiola, D. Hardisson, S.A. Eccles, Advances in establishment and analysis of three-dimensional tumor spheroid-based functional assays for target validation and drug evaluation, BMC Biol. 10 (1) (2012) 1–21, https://doi.org/10.1186/1741-7007-10-29.
[59] A.S. Nunes, A.S. Barros, E.C. Costa, A.F. Moreira, I.J. Correia, 3D tumor spheroids as in vitro models to mimic in vivo human solid tumors resistance to therapeutic drugs, Biotechnol.Bioeng. 116 (1) (2019) 206–226, https://doi.org/10.1002/bit.26845.